A novel method to derive the aerosol hygroscopicity parameter based only on measurements from a humidified nephelometer system

Ye Kuang[1], ChunSheng Zhao[1], JiangChuan Tao[1], YuXuan Bian[2], Nan Ma[3], Gang Zhao[1]

[1]{Department of Atmospheric and Oceanic Sciences, School of Physics, Peking University, Beijing, China}

[2]{State Key Laboratory of Severe Weather, Chinese Academy of Meteorological Sciences}

[3]{Leibniz Institute for Tropospheric research, Leipzig, Germany}

*Correspondence to: C. S. Zhao (zcs@pku.edu.cn)

Abstract

Aerosol hygroscopicity is crucial for understanding roles of aerosol particles in atmospheric chemistry and aerosol climate effects. Light scattering enhancement factor $f(\mathrm{RH},\lambda)$ is one of the parameters describing aerosol hygroscopicity which is defined as $f(\mathrm{RH},\lambda) = \sigma_{sp}(RH,\lambda)/\sigma_{sp}(dry,\lambda)$ where $\sigma_{sp}(RH,\lambda)$ or $\sigma_{sp}(dry,\lambda)$ represents σ_{sp} at wavelength λ under certain RH or dry conditions. Traditionally, an overall hygroscopicity parameter κ can be retrieved from measured $f(\mathrm{RH},\lambda)$, hereinafter referred to as $\kappa_{f(\mathrm{RH})}$, by combining concurrently measured particle number size distribution (PNSD) and mass concentration of black carbon. In this paper, a new method is proposed to directly derive $\kappa_{f(\mathrm{RH})}$ based only on measurements from a three-wavelength humidified nephelometer system. The advantage of this newly proposed approach is that $\kappa_{f(\mathrm{RH})}$ can be estimated without any additional information about PNSD and black carbon. This method is verified with measurements from two different field campaigns. Values of $\kappa_{f(\mathrm{RH})}$ estimated from this new method agree very well with those retrieved by using the traditional method, all points lie nearby 1:1 line, the square of correlation coefficient between them is 0.99. The verification results demonstrate that this newly proposed method of deriving $\kappa_{f(\mathrm{RH})}$ is applicable in different sites and seasons of the North China Plain and might be also applicable in other regions around the world.

1. Introduction

Atmospheric aerosol particles play vital roles in visibility, energy balance and the hydrological cycle of the Earth-atmosphere system and have attracted a lot of attention in recent decades. Aerosol particles suspended in the atmosphere directly influence radiative transfer of solar radiation and indirectly affect cloud properties, therefore, have large impacts on climate change. Especially, uncertainties in direct aerosol radiative forcing due to anthropogenic aerosols and in aerosol indirect forcing caused by aerosol interaction with clouds contribute most to the total uncertainty in climate forcing (Boucher et al., 2013). One of the most important factors affect these uncertainties is the interaction between aerosol particles and ambient atmospheric water vapour (Zhao et al., 2006;Kuang et al., 2016b). Under supersaturated conditions, aerosol particles serve as cloud condensation nuclei (CCN) and hence influence cloud properties. Under subsaturated conditions, with respect to typical aerosol compositions, water usually constitutes about half of the aerosol mass at a relative humidity (RH) of 80% with substantially higher water mass fractions existing at RH values above 90% for most ambient aerosol (Bian et al., 2014).The water content of aerosol and cloud droplets depend on both the ambient RH and hygroscopicity of the aerosol chemical constituents.

Traditionally, the K*ö*hler theory (Petters and Kreidenweis, 2007) is widely used to describe the hygroscopic growth of aerosol particles and successfully used in laboratory studies for single component and some multicomponent particles. In order to account for the mixed organic and inorganic composition of ambient aerosol, Petters and Kreidenweis (2007) proposed a modified version of K*ö*hler theory called κ-K*ö*hler theory to describe a single aerosol hygroscopic growth parameter, κ. The κ-K*ö*hler equation, expressed in terms of the diameter growth factor, g(RH), is given in equation (1) below:

$$\frac{RH}{100} = \frac{g^3-1}{g^3-(1-\kappa)} \cdot \exp\left(\frac{4\sigma_{s/a} \cdot M_{water}}{R \cdot T \cdot D_d \cdot g \cdot \rho_w}\right) \quad (1)$$

where g corresponds to g(RH), D_d is the dry diameter, $\sigma_{s/a}$ is the surface tension of solution/air interface, T is the temperature, M_{water} is the molecular weight of water, R is the universal gas constant, ρ_w is the density of water, and κ is the hygroscopicity parameter. This theory is not only applicable to single-component aerosol particles, but also to multicomponent aerosol particles. With regard to a multicomponent aerosol particle, the Zdanovskii, Stokes, and Robinson assumption can be applied. The hygroscopicity parameter κ of multicomponent aerosol particle can be derived by

using the following formula: $\kappa = \sum_i \varepsilon_i \cdot \kappa_i$, where κ_i and ε_i represent the hygroscopic parameter and volume fraction of each component. This hygroscopicity parameter κ has received much attentions and turns out to be a very effective parameter to study aerosol hygroscopicity. This hygroscopicity parameter κ makes the comparison of the aerosol hygroscopicity at different sites around the world and different time periods more convenient. In addition, hygroscopicity parameter κ also facilitates the intercomparison of aerosol hygroscopicity derived from different techniques and measurements made at different RHs. This hygroscopicity parameter κ is widely used to account the influence of aerosol hygroscopic growth on aerosol optical properties as well as aerosol liquid water contents (Tao et al., 2014;Kuang et al., 2015;Brock et al., 2016;Bian et al., 2014;Zieger et al., 2013) and to examine the role of aerosol hygroscopicty in CCN (Chen et al., 2014;Gunthe et al., 2009;Ervens et al., 2010). The derived κ values from field campaigns and laboratory studies will further our understanding in aerosol hygroscopicity and help estimate the influences of aerosol hygroscopic growth on different aspects of atmospheric processes.

The Humidity Tandem Differential mobility Analyzer (HTDMA) measures the aerosol diameter hygroscopic growth as a function of RH. The aerosol hygroscopicity parameter κ can be directly derived from measurements of HTDMA by applying equation (1) (Liu et al., 2011;Wu et al., 2016). HTDMA systems can provide insights into the aerosol hygroscopicity at different aerosol diameters, however, they can only be used to derive aerosol hygroscopicity parameter κ within certain size range (usually less than 300 nm). HTDMA systems are not capable of providing more details about aerosol hygroscopicity of aerosol particles which contribute most to aerosol optical properties and aerosol liquid water contents (their diameters usually ranging from 200 nm to 1μm) (Ma et al., 2012;Bian et al., 2014). The effect of aerosol water uptake on the aerosol particle light scattering (σ_{sp}) is usually measured with a humidified nephelometer system. Measurements from a humidified nephelometer system can also be used to calculate the aerosol hygroscopicty parameter κ if the dry aerosol particle number size distribution (PNSD) is measured simultaneously (Chen et al., 2014). The scattering enhancement factor $f(\mathrm{RH},\lambda)$, defined as $f(\mathrm{RH},\lambda) = \sigma_{sp}(RH,\lambda)/\sigma_{sp}(dry,\lambda)$, characterizes changes in the aerosol scattering coefficient with RH, $\sigma_{sp}(RH,\lambda)$ or $\sigma_{sp}(dry,\lambda)$ represents σ_{sp} at wavelength λ at a certain RH or under dry conditions. In this research, $f(\mathrm{RH})$ is referred to as $f(\mathrm{RH}, 550\ \mathrm{nm})$. The nephelometer measures aerosol optical properties of the entire aerosol size distribution. Thus, κ calculated from $f(\mathrm{RH})$ measurements can be understood as an optically

weighted κ and represents the overall hygroscopicty of ambient aerosol particles. This κ is more suitable for being used to account the influences of aerosol hygroscopic growth on aerosol optical properties compared to aerosol hygroscopicity derived from HTDMA and CCN measurements. Traditionally, derivation of κ from f(RH) measurements requires aerosol PNSD as well as black carbon (BC) measurements to determine the imaginary part of the refractive index. As PNSD and BC measurements are expensive, their availability in field campaigns are limited.

In this paper we use measurements from a field campaign on the North China Plain (NCP) to derive κ values using 3 methods. The first 2 methods derive κ from aerosol diameter hygroscopic growth and the third method derives an aerosol optical parameterization of κ. Method 1, labeled as $\kappa_{f(RH)}$, derives κ from aerosol PNSD, BC and nephelometer f(RH) measurements. Method 2, defined as κ_{250}, derives κ from g(RH) measurements of aerosol particles with diameter of 250 nm, using a High-Humidity Differential Mobility Analyzer (HH-TDMA). HH-TDMA is a system very similar to HTDMA but is capable of operating at higher RH points (Liu et al., 2011). Method 3, defined as κ_{sca}, is an empirical determination of κ using only nepehelometer measurements of the aerosol scattering coefficient as a function of RH.

Based on detailed analysis about the relationship between $\kappa_{f(RH)}$ and κ_{sca}, a novel method to directly derive $\kappa_{f(RH)}$ based only on measurements from a humidified nephelometer system is proposed. This newly proposed approach makes it more convenient and cheaper for researchers to conduct aerosol hygroscopicity research with $f(\mathrm{RH})$ measurements.

2. Site description and instruments

Datasets from five field campaigns are used in this paper. The five campaigns are conducted at four different measurement sites of the North China Plain (NCP) (Wangdu, Xianghe and Gucheng in Hebei province and Wuqing in Tianjin, and site locations are shown in Fig.S1). Time periods and used datasets from these filed campaigns are listed in Table 1.

During these field campaigns, sampled aerosol particles have aerodynamic diameters less than 10 μm (selected by passing through an impactor). Aerosol PNSDs with particle diameter ranging from 3nm to 10μm were jointly measured by a Twin Differential Mobility Particle Sizer (TDMPS, Leibniz-Institute for Tropospheric Research (IfT), Germany; Birmili et al. (1999)) or a scanning mobility particle size spectrometer (SMPS) and an Aerodynamic Particle Sizer (APS, TSI Inc., Model 3321)

with a temporal resolution of 10 minutes. The mass concentrations of BC were measured using a Multi-angle Absorption Photometer (MAAP Model 5012, Thermo, Inc., Waltham, MA USA) or an aethalometer called AE33 (Drinovec et al., 2015). The aerosol light scattering coefficients (σ_{sp}) at three wavelengths were measured using a TSI 3563 nephelometer (Anderson and Ogren, 1998) or an Aurora 3000 nephelometer (Müller et al., 2011).

A humidified nephelometer system consists of two nephelometers and a humidifier was used in Wangdu and Gucheng campaigns. For the humidified nephelometer systems that we have designed, they only scan the hydration branch of the aerosol hygroscopic growth. The humidifier humidified the sample air through a Gore-Tex tube. The water vapor penetrates through the Gore-Tex tube, which is surrounded by a circulating water layer in a stainless steel tube. The temperature cycle of the circulating water layer was specified and controlled by a water bath. During Wangdu campaign, only one water bath was used, for each RH scanning cycle, the temperature cycle was fixed. Thus, the RH range of each cycle will change. Since the room temperature of the container was relatively stable during Wangdu campaign, the RH points of $f(\mathrm{RH})$ cycles range from about 50% to about 90%, and each cycle lasted about 45 minutes. However, one cycle cost about 90 minutes because after each cycle was finished, the water bath needed about another 45 minutes to cool. During Gucheng campaign, this problem is solved by using two water baths and they provided circulating water alternatively for the humidifier. The corresponding temporal resolution of $f(\mathrm{RH})$ cycles was about 45 minutes. In addition, a control software system was developed and can make sure the RH scans within certain RH range. During Gucheng campaign, the RH points of each $f(\mathrm{RH})$ cycle range from 45% to 90%. During Wangdu campaign, the two nephelometers operated in series, used nephelometer was TSI 3563. During Gucheng campaign, the two nephelometers operated in parallel, used nephelometer was Aurora 3000. In the following, we refer the nephelometer which measures σ_{sp} in dry state and the nephelometer which measures σ_{sp} at different RH points as dry Neph and wet Neph, respectively. Two combined RH and temperature sensors (Vaisala HMP110; accuracy of ± 0.2 ℃ and ± 1.7 % for RH ranges from 0 to 90 %, respectively, and accuracy of ± 2.5 % for RH ranges from 90 % to 100 % according to the manufacturer) are placed at the inlet and outlet of the wet Neph, and the measured RHs and temperatures are defined as RH_1/T_1 and RH_2/T_2, respectively. The dew points at the inlet and outlet of wet Neph were calculated using the measured RH_1/T_1 and RH_2/T_2, and the average value was considered as the dew point of the sample air. The sample RH can be calculated

through the derived dew point and the sample temperature which is measured by the sensor inside the sample cavity of the nephelometer. During Wangdu campaign, measurements from the humidified nephelometer system were only available from 21 June, 2014, to 1 July , 2014. During the two campaigns, the two nephelometers were calibrated every two weeks. The manufacturer of HMP110 suggests that the sensors should be calibrated yearly. We didn't calibrate the used HMP110 sensors during the two campaigns because they only have been used less than three months, and results of cross checks showed that they agree well with each other. The sample RHs in the dry Neph were about 20% and about 8% during Wangdu and Gucheng campaigns, respectively.

Dataset includes aerosol PNSDs at dry state, mass concentrations of BC and σ_{sp} values of different wavelengths from the following four campaigns which are listed in Table 1 are referred to as dataset D1: two campaigns conducted in Wuqing, Xianghe campaign, Wangdu campaign before 21 June, 2014. Note that measured σ_{sp} values of dataset D1 are not corrected for angular truncation errors. This is because that dataset D1 is used for producing the look up table of the newly proposed method, and it is expected that the Ångström exponent calculated from measured σ_{sp} values can be directly used as input for the newly proposed method. However, for σ_{sp} values shown in Fig.1, the angular truncation errors are corrected using Mie theory with measured PNSD and mass concentrations of BC.

During Wangdu campaign, the growth factors of aerosol particles at six selected particle diameters (30 nm, 50 nm, 100 nm, 150nm, 200 nm and 250 nm) at 98% RH condition were obtained from the measurements of the HH-TDMA (Leibniz-Institute for Tropospheric Research (IfT), Germany; Hennig et al. (2005)). Detailed information about HH-TDMA measurements please refer to Liu et al. (2011)

3. Methodology

3.1 Calculations of hygroscopicity parameter κ from $f(\mathbf{RH})$ measurements

Research of Chen et al. (2014) demonstrated that if the PNSD at dry state is measured, then measurements of $f(\mathrm{RH})$ can be used to derive the aerosol hygroscopicity parameter κ by conducting an iterative calculation with the Mie theory and the κ-Köhler theory. To reduce the influence of random errors of observed $f(\mathrm{RH})$ at a certain RH, all valid $f(\mathrm{RH})$ measurements in a complete humidifying cycle is used in the derivation algorithm. The retrieved κ is the κ value which can be used to best fit the observed $f(\mathrm{RH})$ curve, labelled as $\kappa_{f(RH)}$, and this method of deriving κ

is Method 1. Details about this retrieval algorithm is described in Chen et al. (2014). Of particular note is that in this research the mass concentration of BC is also considered in the retrieval algorithm to account for the influence of BC on refractive indices of aerosol particles at different sizes. During the simulating process, aerosol components are divided into two classes in terms of their optical properties: the light absorbing component (i.e. BC) and less absorbing components (comprising inorganic salts and acids such as sulfates, nitrates, ammoniums, as well as most of the organic compounds). The BC is considered to be homogeneously mixed with other aerosol components, and the mass size distribution of BC used in Ma et al. (2012) which is observed on the NCP is used in this research to account the mass distributions of BC at different particle sizes. The used refractive index and density of BC are $1.80 - 0.54\mathrm{i}$ and $1.5\mathrm{g}\,cm^{-3}$ (Kuang et al., 2015). Used refractive indices of non light-absorbing aerosol components (other than BC) and liquid water are $1.53 - 10^{-7}i$ (Wex et al., 2002) and $1.33 - 10^{-7}i$ (Seinfeld and Pandis, 2006), respectively. The flow chart about this retrieval algorithm is also introduced in the supporting information, please refer to Fig.S2 for more details.

3.2 Calculations of hygroscopicity parameter κ from HH-TDMA measurements

The HH-TDMA measures hygroscopic growth factors of particles at different sizes at 98% RH condition. The measured hygroscopic factors can be directly related to κ with equation (1). For a specified size of selected aerosol particles, a distribution of growth factors can be measured, and thus can be used to derive a probability distribution of κ and finally come to the calculation of average κ value corresponding to this size of aerosol particles. The method on how to derive average κ value of certain size of aerosol particles from HH-TDMA measurements is elaborately described in Liu et al. (2011). In this research κ values derived from g(RH) measurements of aerosol particles with diameter of 250 nm are used, defined as κ_{250}. This method of deriving κ is Method 2.

3.3 Parameterization schemes for $f(\mathrm{RH})$

The most frequently used $f(\mathrm{RH})$ parameterization scheme is a power-law function which is known as "gamma" parameterization (Hänel, 1981) and the formula of this single-parameter representation is written as the following:

$$f(\mathrm{RH}) = \left[\frac{100-RH_0}{100-RH}\right]^{\gamma} \quad (2)$$

where RH_0 is the RH of dry condition, and γ is a parameter fitted to the observed $f(\mathrm{RH})$. In this study, we estimated γ values with observed $f(\mathrm{RH})$ curves and for the first time to our knowledge,

206 we further examined the relationship between γ and $\kappa_{f(RH)}$.

207 Recently, a new physically based single-parameter representation was proposed by Brock et al.
208 (2016) to describe $f(\mathrm{RH})$. Their results demonstrated that this proposed parameterization scheme can
209 better describe $f(\mathrm{RH})$ than the widely used gamma power-law approximation (Brock et al., 2016).
210 The formula of this new scheme is written as:

211 $$f(\mathrm{RH}) = 1 + \kappa_{sca}\frac{RH}{100-RH} \qquad (3)$$

212 where κ_{sca} is a parameter fits $f(\mathrm{RH})$ best. Regardless of the curvature effects for particle diameters
213 larger than 100 nm, the hygroscopic growth factor for aerosol particles can be approximately expressed
214 as the following (Brock et al., 2016): $gf_{diam} \cong (1 + \kappa\frac{RH}{100-RH})^{1/3}$. Moreover, σ_{sp} is usually
215 approximately proportional to total aerosol volume (Pinnick et al., 1980) which means that the relative
216 change in σ_{sp} due to aerosol water uptake is roughly proportional to relative change in aerosol volume.
217 The enhancement factor in volume can be expressed as the cube of gf_{diam}, thus lead to the formula
218 form of $f(\mathrm{RH})$ expressed in equation (3).

219 During processes of measuring $f(\mathrm{RH})$, the sample RH in the dry Neph (RH_0) is not zero.
220 According to equation (3), the measured $f(\mathrm{RH})_{measure} = \frac{f(\mathrm{RH})}{f(RH_0)}$ should be fitted using the following
221 formula:

222 $$f(\mathrm{RH})_{measure} = (1 + \kappa_{sca}\frac{RH}{100-RH})/(1 + \kappa_{sca}\frac{RH_0}{100-RH_0}) \qquad (4)$$

223 The method of calculating κ_{sca} by curve fitting using equation (4) is called Method 3. The
224 "gamma" parameterization scheme is referred to as γ-Method in the following paragraphs.

225 **4. Results and discussions**

226 **4.1 Derived κ values from $f(\mathrm{RH})$ and HH-TDMA measurements**

227 During this field campaign, the aerosol physical, chemical and optical properties are
228 synergistically observed with different types of instruments. They provide valuable datasets to perform
229 an insightful analysis about aerosol hygroscopicity and its relationship with other aerosol properties.
230 The time series of σ_{sp} at 550 nm at dry state are shown in Fig.1a.. The results show that this
231 observation period has experienced varying degrees of pollution levels, with σ_{sp} at 550 nm ranging
232 from 15 to 1150 Mm^{-1}.Values of $\kappa_{f(\mathrm{RH})}$ derived from Method 1 are shown in Fig.1b. During
233 deliquescence f(RH) exhibits an abrupt increase between RH values of 60-65%. As such, only f(RH)

data points with RH >70% were used in determination of $\kappa_{f(\mathrm{RH})}$ when deliquescence was apparent. For f(RH) cycles without deliquescence, all f(RH) points are used in the retrieval algorithm with RH ranges of about 50% to 90%. The results demonstrate that $\kappa_{f(\mathrm{RH})}$ lies between 0.06 and 0.51, with an average of 0.32. The lowest $\kappa_{f(\mathrm{RH})}$ values are found when the air quality is relatively clean (σ_{sp} at 550 nm is lower than 100 Mm^{-1}) on 27 and 28 June. During these two days, organic matter dominates the mass concentration of PM2.5 which results in the low hygroscopicity of aerosol particles (Kuang et al., 2016a). On the contrary, the largest $\kappa_{f(\mathrm{RH})}$ values are found during periods when deliquescent phenomena occur and inorganic chemical compositions dominate the mass concentrations of PM2.5, especially, sulfate is highly abundant during these periods. Of particular note is that during relatively polluted periods (σ_{sp} at 550 nm larger than 100 Mm^{-1}) aerosol particles are generally very hygroscopic which imply that aerosol water uptake can exert significant impacts on regional direct aerosol radiative effect and ambient visibility during this observation period.

On the basis of the average size-resolved κ distribution from Haze in China (HaChi) campaign (Liu et al., 2014), κ values change a lot for aerosol particles whose diameters are less than 250 nm, however, κ values vary relatively smaller for aerosol particles whose diameter range from 250 nm to 1 μm. In addition, the results from HaChi campaign also demonstrate that aerosol particles whose diameter range from 200 nm to 1 μm usually contribute more than 80% to σ_{sp} at 550 nm during summer on the NCP (Ma et al., 2012). That is, $\kappa_{f(\mathrm{RH})}$ may share similar magnitude with κ_{250}. To compare κ values derived from Method 1 and Method 2values of κ_{250} are also shown in Fig.1b. During this observation period, values of κ_{250} range from 0.11 to 0.56, with an average of 0.34 which is very close to average κ_{250} observed during HaChi campaign (Liu et al., 2011). The results shown in Fig.1b suggest that, in general, $\kappa_{f(\mathrm{RH})}$ values agree well with κ_{250} values, however, are usually lower than κ_{250} values. To quantitatively compare these two types of κ values, they are plotted against each other and shown in Fig.2. It can be seen that they are highly correlated but overall, the κ_{250} values are higher than $\kappa_{f(\mathrm{RH})}$ values, and the average difference between κ_{250} and $\kappa_{f(\mathrm{RH})}$ is 0.02. The statistical relationship between κ_{250} and $\kappa_{f(\mathrm{RH})}$ is also shown in Fig.2.This relationship may be useful for researchers if they want to estimate the influences of aerosol water uptake on aerosol optical properties and aerosol liquid water contents when only HH-TDMA or HTDMA measurements are available.

A model experiment is conducted to better understand the relationship between κ_{250} and $\kappa_{f(\mathrm{RH})}$. During HaChi campaign, size-resolved κ distributions are derived from measured size-segregated chemical compositions (Liu et al., 2014) and their average is used in this experiment to account the size dependence of aerosol hygroscopicity which is shown in Fig. 3a. With this fixed average size-resolved κ distribution, all observed PNSDs at dry state along with mass concentrations of BC from dataset D1 are used to simulate the retrieval of $\kappa_{f(\mathrm{RH})}$ under different PNSD and BC conditions. The used PNSDs shown in Fig.3b indicate that large varying types of PNSDs are considered in the simulative experiment. As to the simulating process, with given PNSD, mass concentration of BC and size-resolved κ distribution. The first step is simulating $f(\mathrm{RH})$ points using Mie theory and κ-Köhler theory with RH range of 50% to 90% and the RH interval is 10%. The second step is retrieving corresponding $\kappa_{f(\mathrm{RH})}$ using the procedure of Method 1. The κ value at particle diameter of 250 nm of the used size-resolved κ distribution is the corresponding κ_{250}. The probability distribution of simulated $\kappa_{f(\mathrm{RH})}$ is also shown in Fig.3a. The standard deviation of retrieved $\kappa_{f(\mathrm{RH})}$ is about 0.01 which suggests that if the size-resolved κ distribution is fixed, then $\kappa_{f(\mathrm{RH})}$ varies little. Due to $\kappa_{f(\mathrm{RH})}$ represents an overall, size-integrated κ, it is clearly shown in Fig.3a that in most cases $\kappa_{f(\mathrm{RH})}$ values are located between κ values of aerosol particles ranging from 200 nm to 1μm. Moreover, about 70% of simulated $\kappa_{f(\mathrm{RH})}$ values are less than κ_{250} which to some extent explains the observed difference between κ_{250} and $\kappa_{f(\mathrm{RH})}$ mentioned before. However, the simulated average difference between κ_{250} and average $\kappa_{f(\mathrm{RH})}$ is about 0.01 which is less than the observed averaged difference between κ_{250} and $\kappa_{f(\mathrm{RH})}$ which is 0.02. Especially, when $\kappa_{f(\mathrm{RH})}$ values are relatively lower ($<$ 0.25), the κ_{250} is systematically higher than $\kappa_{f(\mathrm{RH})}$. Except that uncertainties from measurements of instruments, for example, the uncertainty of RH in measurements of HH-TDMA and uncertainties of measuring $f(\mathrm{RH})$ (details about the uncertainty sources of $f(\mathrm{RH})$ measurements can be found in the paper published by Titos et al. (2016)), there are other two reasons may be associated with the discrepancy between κ_{250} and $\kappa_{f(\mathrm{RH})}$. The first one is that configurations of size-resolved κ distributions and PNSDs during this field campaign are far different from the model experiment. The second one is that in the real atmosphere, κ values at different RH conditions may be different (You et al., 2014) and most of $f(\mathrm{RH})$ measurements are conducted when RH is lower than 90%, however, the measurements of HH-TDMA are conducted when RH is equal to 98% . Overall, the observed general consistency between κ values derived from measurements of $f(\mathrm{RH})$ and HH-TDMA

confirms the reliability of κ values derived from $f(\mathrm{RH})$ measurements.

4.2 Relationships between κ derived from $f(\mathrm{RH})$ measurements and $f(\mathrm{RH})$ fitting parameters

In the previous section, derived $\kappa_{f(\mathrm{RH})}$ values are characterized and compared with κ_{250} values. These results demonstrated that derived $\kappa_{f(\mathrm{RH})}$ values can commendably represent variations of aerosol hygroscopicty of ambient aerosol populations. In this section, the relationship between derived $\kappa_{f(\mathrm{RH})}$ values and $f(\mathrm{RH})$ fitting parameters are further examined to investigate their relationships.

Two parameterization schemes of $f(\mathrm{RH})$ are discussed in this paper, including the γ-Method and Method 3. Values of γ and κ_{sca} are fitted from observed $f(\mathrm{RH})$ cycles. For cycles during deliquescent periods, only $f(\mathrm{RH})$ points with RH higher than 70% are used to perform fitting processes. The relationship between $\kappa_{f(\mathrm{RH})}$ and γ is investigated and shown in Fig.4a. It is found that an approximately linear relationship exists (square of correlation coefficient is 0.90) between $\kappa_{f(\mathrm{RH})}$ and γ, especially when $\kappa_{f(\mathrm{RH})}$ is larger than 0.2. During this field campaign, fitted γ ranges from 0.13 to 0.56 with an average of 0.41.

During this field campaign, fitted κ_{sca} ranges from 0.05 to 0.36 with an average of 0.22. The relationship between $\kappa_{f(\mathrm{RH})}$ and κ_{sca} is also investigated and shown in Fig.4b. It is found that a strong linear relationship also exists (square of correlation coefficient is 0.97) between $\kappa_{f(\mathrm{RH})}$ and κ_{sca}. The statistically fitted line almost passes though zero point which implies that a proportional relationship may exist between $\kappa_{f(\mathrm{RH})}$ and κ_{sca}. This strong correlation should be intrinsic due to the idea of Method 3 is from the linkage between total aerosol volume and σ_{sp} as introduced in Sect.3.3 and the increase of total aerosol volume due to aerosol water uptake is directly linked to the overall aerosol hygroscopicity parameter κ. It seems that this promising linear relationship can help bridge the gap between $f(\mathrm{RH})$ and κ. However, results from Brock et al. (2016) imply that the relationship between $\kappa_{f(\mathrm{RH})}$ and κ_{sca} is much more sophisticated and it is affected by both aerosol hygroscopicity and PNSD at dry state. In the paper published by Brock et al. (2016), κ_{ext} (a parameter determined from measurements of the aerosol extinction coefficient as a function of RH using formula form of equation (2)) and κ_{chem} (a constant κ determined from chemical constituents of entire aerosol population) are used and correspond to κ_{sca} and $\kappa_{f(\mathrm{RH})}$ in this research, the difference between κ_{ext} and κ_{sca} is that κ_{ext} is used to fit the light enhancement factor of aerosol extinction

coefficient, κ_{chem} and $\kappa_{f(\mathrm{RH})}$ actually means the same because both them are overall and size independent hygroscopicity parameters. Results from Brock et al. (2016) concluded that the ratio $\kappa_{ext}/\kappa_{chem}$ generally lies between 0.6 to 1 which implies that the ratio $\kappa_{sca}/\kappa_{f(\mathrm{RH})}$ (in the following, this ratio is referred to as R_κ) also should have large variations and may share a similar range of variability. By revisiting the relationship between $\kappa_{f(\mathrm{RH})}$ and κ_{sca} found in this research, it can be found that R_κ during this field campaign ranges from 0.58 to 0.77 with an average of 0.69. This result suggests that if we directly establish a linkage between $\kappa_{f(\mathrm{RH})}$ and κ_{sca} with an average R_κ can result in a non-negligible bias (relative difference can reach about 15%). Besides, this range of R_κ only represents the relationship between $\kappa_{f(\mathrm{RH})}$ and κ_{sca} during a short time period and at only one site.

To better understand the relationship between $\kappa_{f(\mathrm{RH})}$ and κ_{sca}, all PNSDs at dry state (shown in Fig.3a) along with mass concentrations of BC from dataset D1 are used to simulate the relationship between $\kappa_{f(\mathrm{RH})}$ and κ_{sca} with Mie and κ-K*ö*hler theories. The aim of including PNSD and BC information from different campaigns is to simulate variations of R_k under different conditions. During simulating processes, for each PNSD, we change $\kappa_{f(\mathrm{RH})}$ from 0.01 to 0.7 with an interval of 0.01 to examine the influence of aerosol hygroscopicity on R_κ. For each PNSD and $\kappa_{f(\mathrm{RH})}$, the simulating processes include two steps. The first step is simulating $f(\mathrm{RH})$ points using Mie theory and κ-K*ö*hler theory with RH range of 50% to 90% and the RH interval is 10%. The way of treating BC is same with the retrieval procedure of $\kappa_{f(\mathrm{RH})}$ introduced in Sect.3.1. The second step is retrieving the corresponding $\kappa_{f(\mathrm{RH})}$ using the procedure of Method 1 and calculating κ_{sca} with Method 3. Simulated results of $\kappa_{f(\mathrm{RH})}$ and κ_{sca} are shown in Fig.5a and the probability distribution of corresponding R_κ values is shown in Fig.5b. The results show that R_κ primarily ranges from 0.5 to 0.84 with an average of 0.69 which is same with the average R_κ measured during Wangdu campaign. These results also indicate that the relationship between $\kappa_{f(\mathrm{RH})}$ and κ_{sca} is much more complex than a simple linear relationship and more information about aerosol properties are necessary to gain insights into the variation of R_κ.

4.3 A novel method to directly derive κ from measurements of a humidified nephelometer system

A robust linear relationship is found between $\kappa_{f(\mathrm{RH})}$ and κ_{sca} in Sect.4.2 , however, results of further analysis suggest that R_κ varies a lot. The complexity comes from that both PNSD at dry

state and aerosol hygroscopicity have impacts on R_κ. Generally, used nephelometer of a humidified nephelometer system have three wavelengths (Titos et al., 2016) and the spectral dependence of σ_{sp} is usually described by the following Ångström formula: $\sigma_{sp}(\lambda) = \beta\lambda^{-\alpha_{sp}}$, where β is the particle number concentration dependent coefficient, λ is the wavelength of light and α_{sp} represents the Ångström exponent of σ_{sp}. Ångström exponent can be directly inferred from the measurements of σ_{sp} at different wavelengths. Of particular note is that Ångström exponent not only can be used to account the spectral course of σ_{sp}, it also reveals information about PNSD. In general, larger value of Ångström exponent corresponds to smaller aerosol particles. That is, Ångström exponent can be a proxy of PNSD at dry state and be used in the processes of estimating the impacts of PNSD on R_κ. On the other hand, with regard to aerosol hygroscopicity, although R_κ varies within certain range, value of κ_{sca} can still be used to represent the overall hygroscopicity of aerosol particles.

Simulated R_κ values introduced in the last paragraph of Sect.4.2 are spread into a two dimensional gridded plot, they are simulated from all observed PNSDs and mass concentrations of BC of dataset D1. The first dimension is Ångström exponent with an interval of 0.02 and the second dimension is κ_{sca} with an interval of 0.01, average R_κ value within each grid is represented by color and shown in Fig.6a. Values of Ångström exponent corresponding different PNSDs are calculated from concurrently measured σ_{sp} values at 450 nm and 550 nm from TSI 3563 nephelometer. Based on results shown on Fig.6a, the different impacts of aerosol hygroscopicity and dry scattering Ångström exponent on R_κ can be distinguished to some extent. The results demonstrate that PNSD at dry state play a more important role in the variations of R_κ than overall aerosol hygroscopicty.. Overall, larger value of Ångström exponent corresponds to higher R_κ. Aerosol hygroscopicty exhibits different influences on R_κ when Ångström exponent values are different. On average, higher κ_{sca} corresponds to lower R_κ if Ångström exponent is smaller than about 0.8 and higher κ_{sca} corresponds to higher R_κ if Ångström exponent is larger than about 1.6.The percentile value of standard deviation of R_κ values within each grid of Fig.6a divided by their average is shown in Fig.6b. The Ångström exponent only represents an overall size property of aerosol particles, the same Ångström exponent corresponds to different aerosol PNSDs. Within each grid of Fig.6a, the same κ_{sca} corresponds to different combinations of aerosol PNSD and $\kappa_{f(\mathrm{RH})}$, and R_κ values also change. Note that the size-dependent chemical composition also exerts influence on R_k. However, if

PNSD is fixed, each size-resolved κ distribution corresponds to a certain $\kappa_{f(RH)}$, and $\kappa_{f(RH)}$ varies with certain range no matter how size-resolved κ distribution changes. Therefore, influences of size-dependent chemical compositions on R_k are already included in the simulated results of producing the look up table by varying the $\kappa_{f(RH)}$ from 0 to 0.7 for a fixed aerosol PNSD.

As shown in Fig.6b, in most cases, these percentile values are less than 6% (about 80%) which demonstrates that R_κ varies little within each grid shown in Fig.6a. This implies that results of Fig.6a can be used as a look up table to estimate R_κ. As what's introduced before, currently used nephelometer of a humidified nephelometer system usually have three wavelengths (Titos et al., 2016), thus can provide information about Ångström exponent, and κ_{sca} can be directly fitted from observed $f(\mathrm{RH})$ curve. Even only one $f(\mathrm{RH})$ point is measured, κ_{sca} can still be calculated from equation (4). Using results shown in Fig.6a as a look up table, R_κ values can be directly predicted from measurements of a humidified nephelometer system. With this method, R_κ values during this Wangdu field campaign are predicted (values of Ångström exponent are calculated from measured σ_{sp} values at 450 nm and 550 nm under dry conditions) and compared with measured R_κ values, the results are shown in Fig.7a. The Ångström exponent during this field campaign ranges from 0.63 to 1.96 with an average of 1.4. It can be seen from Fig.7a that majority of points lie nearby 1:1 line and 82% points have relative differences less than 6% which is consistent with results shown in Fig.6b. This result is quite promising and can be further used to derive $\kappa_{f(\mathrm{RH})}$ values by combining fitted κ_{sca} and predicted R_κ. This method of deriving $\kappa_{f(\mathrm{RH})}$ is called Method 4 and include two steps. The first step is calculating Ångström exponent based on measured σ_{sp} values at 450 nm and 550 nm by the dry nephelometer and calculating κ_{sca} based on measured $f(\mathrm{RH})$ curve by the humidified nephelometer system. The second step is predicting R_κ using the look up table shown in Fig.6a, and then calculate $\kappa_{f(\mathrm{RH})}$ based on predicted R_κ and fitted κ_{sca}. The results of predicted $\kappa_{f(\mathrm{RH})}$ values are shown in Fig.7b and a robust correlation between $\kappa_{f(\mathrm{RH})}$ values predicted from Method 4 and $\kappa_{f(\mathrm{RH})}$ values derived from Method 1 is achieved (the square of correlation coefficient between them is 0.99). All points shown in Fig.7b lie nearby 1:1 line, average difference between $\kappa_{f(\mathrm{RH})}$ derived from Method 4 and Method 1 is -0.009.

Datasets from Gucheng campaign are further used to verify Method 4. In this campaign, Aurora 3000 nephelometer is used for the humidified nephelometer system, it has three wavelengths: 450 nm,

525 nm and 635 nm. Values of $f(\mathrm{RH},\lambda)$ points correspond to wavelength of 525 nm are used to derive $\kappa_{f(\mathrm{RH})}$ using Method 1 and Method 4, used RH range is 45% to 90%. The look up table shown in Fig.6a is simulated corresponding to scattering wavelength of 550 nm, and is not suitable for being used in Method 4 if the nephelometer is Aurora 3000. A new look up table is simulated corresponding to scattering wavelength of 525 nm, used datasets of PNSD and BC are same with those for producing the look up table shown in Fig.6a. During Gucheng campaign, the variations of $\kappa_{f(\mathrm{RH})}$ and corresponding R_k with σ_{sp} at 525 nm are shown in Fig.8a. Values of $\kappa_{f(\mathrm{RH})}$ range from 0.01 to 0.27, with an average of 0.14. During this campaign, $\kappa_{f(\mathrm{RH})}$ is relatively lower when σ_{sp} is high. Values of R_k range from 0.60 to 0.84, with an average of 0.7. Results of the comparison between $\kappa_{f(\mathrm{RH})}$ derived from Method 1 and Method 4 are shown in Fig.8b. The results demonstrate that good consistency is achieved between $\kappa_{f(\mathrm{RH})}$ derived from Method 1 and Method 4, the square of correlation coefficient between them is 0.99.

The verification results of Method 4 using measurements from Wangdu and Gucheng campaigns demonstrate that a quite good estimation of $\kappa_{f(\mathrm{RH})}$ can be achieved by using only measurements from a humidified nephelometer system. The processes of simulating the look up table are independent of the size-resolved κ distribution, and used PNSDs are from four different field campaigns which were conducted in different sites and seasons of the NCP. The verification datasets from two different field campaigns are totally independent of the look up table and also from different sites and seasons of the NCP. These results demonstrate that the newly proposed method is applicable in different sites and seasons of the NCP. The results shown in Fig.6b demonstrate that if Ångström exponent and κ_{sca} are fixed, then R_k varies little. The maximum κ_{sca} of the look up table is 0.4, if R_k is 0.8 (close to the simulated highest R_k shown in Fig.5b), the corresponding $f(\mathrm{RH}=80\%)$ is 2.6. According to the review of Titos et al. (2016), most of $f(\mathrm{RH}=80\%)$ values for continental aerosols are lower than 2.6. The Ångström exponent range of the look up table is 0.4 to 2.0. Which demonstrate that the look up table shown in Fig.6a already covers large variation ranges of Ångström exponent and κ_{sca} and can be used under different conditions. Thus, the newly proposed method of deriving $\kappa_{f(\mathrm{RH})}$ might be also applicable in other regions around the world. However, it should be pointed out that the look up table shown in Fig.6a is from simulations of measured continental aerosols without influences of desert dust, and it might not be suitable for being used to estimate $\kappa_{f(\mathrm{RH})}$ when sea salt or dust particles prevail. In summary, this approach allows researchers to directly derive aerosol

hygroscopicity from measurements of $f(\mathrm{RH})$ without any additional information about PNSD and BC which is quite convenient for researchers to conduct aerosol hygroscopicity researches with measurements from a humidified nephelometer system.

5. Conclusions

In this paper, values of aerosol hygroscopicity parameter κ during Wangdu campaign are first derived from measurements of $f(\mathrm{RH})$ by combining measurements of PNSD at dry state and BC. The results show that during this field campaign, aerosol hygroscopicity varies a lot, and $\kappa_{f(\mathrm{RH})}$ ranges from 0.06 to 0.51 with an average of 0.34. Retrieved $\kappa_{f(\mathrm{RH})}$ values are further compared with κ_{250} which is derived from measurements of HH-TDMA and good consistency is achieved.

Relationships between $\kappa_{f(\mathrm{RH})}$ and $f(\mathrm{RH})$ fitting parameters γ and κ_{sca} are further investigated in Sect.4.2 which is for the first time to our knowledge. Good linear relationship is found between $\kappa_{f(\mathrm{RH})}$ and κ_{sca} during Wangdu campaign. Results of detailed analysis about the relationship between $\kappa_{f(\mathrm{RH})}$ and κ_{sca} demonstrate that the relationship between $\kappa_{f(\mathrm{RH})}$ and κ_{sca} is complicated, and the ratio $\kappa_{sca}/\kappa_{f(\mathrm{RH})}$ (R_κ) varies a lot (0.5 to 0.84, with an average of 0.69).

In Sect.4.3, a look up table based on Ångström exponent and κ_{sca} is developed to estimate R_κ. With this look up table, R_κ as well as $\kappa_{f(\mathrm{RH})}$ can be directly estimated from measurements of a humidified nephelometer system. This method is further verified with measurements from two different campaigns. The verification results demonstrate that a quite good estimation of $\kappa_{f(\mathrm{RH})}$ can be achieved by using only measurements from a humidified nephelometer system, and this method is applicable at different sites and in different seasons of the NCP and might be also applicable in other regions around the world. This newly proposed novel approach allow researchers to estimate $\kappa_{f(\mathrm{RH})}$ without any additional information about PNSD and BC. This new finding directly links κ and $f(\mathrm{RH})$ and will make the humidified nephelometer system more convenient when it comes to aerosol hygroscopicity research. Finally, findings in this research may facilitate the intercomparison of aerosol hygroscopicity derived from different techniques, help for parameterizing $f(\mathrm{RH})$ and predicting CCN properties with optical measurements.

Acknowledgments

This work is supported by the National Natural Science Foundation of China (41590872, 41375134).

The data used are listed in the references and a repository at http://pan.baidu.com/s/1c2Nzc5a.

References

Anderson, T. L., and Ogren, J. A.: Determining aerosol radiative properties using the TSI 3563 integrating nephelometer, Aerosol Science and Technology, 29, 57-69, 10.1080/02786829808965551, 1998.

Bian, Y. X., Zhao, C. S., Ma, N., Chen, J., and Xu, W. Y.: A study of aerosol liquid water content based on hygroscopicity measurements at high relative humidity in the North China Plain, Atmos. Chem. Phys., 14, 6417-6426, 10.5194/acp-14-6417-2014, 2014.

Birmili, W., Stratmann, F., and Wiedensohler, A.: Design of a DMA-based size spectrometer for a large particle size range and stable operation, Journal of Aerosol Science, 30, 549-553, 10.1016/s0021-8502(98)00047-0, 1999.

Boucher, O., Randall, D., Artaxo, P., Bretherton, C., Feingold, G., Forster, P., Kerminen, V.-M., Kondo, Y., Liao, H., Lohmann, U., Rasch, P., Satheesh, S. K., Sherwood, S., Stevens, B., and Zhang, X. Y.: Clouds and Aerosols, in: Climate Change 2013: The Physical Science Basis. Contribution of Working Group I to the Fifth Assessment Report of the Intergovernmental Panel on Climate Change, edited by: Stocker, T. F., Qin, D., Plattner, G.-K., Tignor, M., Allen, S. K., Boschung, J., Nauels, A., Xia, Y., Bex, V., and Midgley, P. M., Cambridge University Press, Cambridge, United Kingdom and New York, NY, USA, 571–658, 2013.

Brock, C. A., Wagner, N. L., Anderson, B. E., Attwood, A. R., Beyersdorf, A., Campuzano-Jost, P., Carlton, A. G., Day, D. A., Diskin, G. S., Gordon, T. D., Jimenez, J. L., Lack, D. A., Liao, J., Markovic, M. Z., Middlebrook, A. M., Ng, N. L., Perring, A. E., Richardson, M. S., Schwarz, J. P., Washenfelder, R. A., Welti, A., Xu, L., Ziemba, L. D., and Murphy, D. M.: Aerosol optical properties in the southeastern United States in summer – Part 1: Hygroscopic growth, Atmos. Chem. Phys., 16, 4987-5007, 10.5194/acp-16-4987-2016, 2016.

Chen, J., Zhao, C. S., Ma, N., and Yan, P.: Aerosol hygroscopicity parameter derived from the light scattering enhancement factor measurements in the North China Plain, Atmos. Chem. Phys., 14, 8105-8118, 10.5194/acp-14-8105-2014, 2014.

Drinovec, L., Močnik, G., Zotter, P., Prévôt, A. S. H., Ruckstuhl, C., Coz, E., Rupakheti, M., Sciare, J., Müller, T., Wiedensohler, A., and Hansen, A. D. A.: The "dual-spot" Aethalometer: an improved measurement of aerosol black carbon with real-time loading compensation, Atmospheric Measurement Techniques, 8, 1965-1979, 10.5194/amt-8-1965-2015, 2015.

Ervens, B., Cubison, M. J., Andrews, E., Feingold, G., Ogren, J. A., Jimenez, J. L., Quinn, P. K., Bates, T. S., Wang, J., Zhang, Q., Coe, H., Flynn, M., and Allan, J. D.: CCN predictions using simplified assumptions of organic aerosol composition and mixing state: a synthesis from six different locations, Atmos. Chem. Phys., 10, 4795-4807, 10.5194/acp-10-4795-2010, 2010.

Gunthe, S. S., King, S. M., Rose, D., Chen, Q., Roldin, P., Farmer, D. K., Jimenez, J. L., Artaxo, P., Andreae, M. O., Martin, S. T., and Pöschl, U.: Cloud condensation nuclei in pristine tropical rainforest air of Amazonia: size-resolved measurements and modeling of atmospheric aerosol composition and CCN activity, Atmos. Chem. Phys., 9, 7551-7575, 10.5194/acp-9-7551-2009, 2009.

Hänel, G.: An attempt to interpret the humidity dependencies of the aerosol extinction and scattering coefficients, Atmospheric Environment (1967), 15, 403-406, http://dx.doi.org/10.1016/0004-6981(81)90045-7, 1981.

Hennig, T., Massling, A., Brechtel, F. J., and Wiedensohler, A.: A tandem DMA for highly temperature-stabilized hygroscopic

particle growth measurements between 90% and 98% relative humidity, Journal of Aerosol Science, 36, 1210-1223, 10.1016/j.jaerosci.2005.01.005, 2005.
Kuang, Y., Zhao, C. S., Tao, J. C., and Ma, N.: Diurnal variations of aerosol optical properties in the North China Plain and their influences on the estimates of direct aerosol radiative effect, Atmos. Chem. Phys., 15, 5761-5772, 10.5194/acp-15-5761-2015, 2015.
Kuang, Y., Zhao, C. S., Ma, N., Liu, H. J., Bian, Y. X., Tao, J. C., and Hu, M.: Deliquescent phenomena of ambient aerosols on the North China Plain, Geophys. Res. Lett., n/a-n/a, 10.1002/2016GL070273, 2016a.
Kuang, Y., Zhao, C. S., Tao, J. C., Bian, Y. X., and Ma, N.: Impact of aerosol hygroscopic growth on the direct aerosol radiative effect in summer on North China Plain, Atmospheric Environment, 147, 224-233, http://dx.doi.org/10.1016/j.atmosenv.2016.10.013, 2016b.
Liu, H. J., Zhao, C. S., Nekat, B., Ma, N., Wiedensohler, A., van Pinxteren, D., Spindler, G., Müller, K., and Herrmann, H.: Aerosol hygroscopicity derived from size-segregated chemical composition and its parameterization in the North China Plain, Atmos. Chem. Phys., 14, 2525-2539, 10.5194/acp-14-2525-2014, 2014.
Liu, P. F., Zhao, C. S., Göbel, T., Hallbauer, E., Nowak, A., Ran, L., Xu, W. Y., Deng, Z. Z., Ma, N., Mildenberger, K., Henning, S., Stratmann, F., and Wiedensohler, A.: Hygroscopic properties of aerosol particles at high relative humidity and their diurnal variations in the North China Plain, Atmos. Chem. Phys., 11, 3479-3494, 10.5194/acp-11-3479-2011, 2011.
Müller, T., Laborde, M., Kassell, G., and Wiedensohler, A.: Design and performance of a three-wavelength LED-based total scatter and backscatter integrating nephelometer, Atmos. Meas. Tech., 4, 1291-1303, 10.5194/amt-4-1291-2011, 2011.
Ma, N., Zhao, C. S., Müller, T., Cheng, Y. F., Liu, P. F., Deng, Z. Z., Xu, W. Y., Ran, L., Nekat, B., van Pinxteren, D., Gnauk, T., Müller, K., Herrmann, H., Yan, P., Zhou, X. J., and Wiedensohler, A.: A new method to determine the mixing state of light absorbing carbonaceous using the measured aerosol optical properties and number size distributions, Atmos. Chem. Phys., 12, 2381-2397, 10.5194/acp-12-2381-2012, 2012.
Petters, M. D., and Kreidenweis, S. M.: A single parameter representation of hygroscopic growth and cloud condensation nucleus activity, Atmospheric Chemistry and Physics, 7, 1961-1971, 2007.
Pinnick, R. G., Jennings, S. G., and Chýlek, P.: Relationships between extinction, absorption, backscattering, and mass content of sulfuric acid aerosols, Journal of Geophysical Research: Oceans, 85, 4059-4066, 10.1029/JC085iC07p04059, 1980.
Seinfeld, J. H., and Pandis, S. N.: Atmospheric chemistry and physics: from air pollution to climate change, John Wiley & Sons, 2006.
Tao, J. C., Zhao, C. S., Ma, N., and Liu, P. F.: The impact of aerosol hygroscopic growth on the single-scattering albedo and its application on the NO2 photolysis rate coefficient, Atmos. Chem. Phys., 14, 12055-12067, 10.5194/acp-14-12055-2014, 2014.
Titos, G., Cazorla, A., Zieger, P., Andrews, E., Lyamani, H., Granados-Muñoz, M. J., Olmo, F. J., and Alados-Arboledas, L.: Effect of hygroscopic growth on the aerosol light-scattering coefficient: A review of measurements, techniques and error sources, Atmospheric Environment, 141, 494-507, http://dx.doi.org/10.1016/j.atmosenv.2016.07.021, 2016.
Wex, H., Neususs, C., Wendisch, M., Stratmann, F., Koziar, C., Keil, A., Wiedensohler, A., and Ebert, M.: Particle scattering, backscattering, and absorption coefficients: An in situ closure and sensitivity study, Journal of Geophysical Research-Atmospheres, 107, 18, 10.1029/2000jd000234, 2002.
Wu, Z. J., Zheng, J., Shang, D. J., Du, Z. F., Wu, Y. S., Zeng, L. M., Wiedensohler, A., and Hu, M.: Particle hygroscopicity and its link to chemical composition in the urban atmosphere of Beijing, China, during summertime, Atmos. Chem. Phys., 16, 1123-1138, 10.5194/acp-16-1123-2016, 2016.
You, Y., Smith, M. L., Song, M., Martin, S. T., and Bertram, A. K.: Liquid–liquid phase separation in atmospherically relevant particles consisting of organic species and inorganic salts, International Reviews in Physical Chemistry, 33, 43-77, 10.1080/0144235X.2014.890786, 2014.

Zhao, C., Tie, X., and Lin, Y.: A possible positive feedback of reduction of precipitation and increase in aerosols over eastern central China, Geophys. Res. Lett., 33, L11814, 10.1029/2006GL025959, 2006.
Zieger, P., Fierz-Schmidhauser, R., Weingartner, E., and Baltensperger, U.: Effects of relative humidity on aerosol light scattering: results from different European sites, Atmos. Chem. Phys., 13, 10609-10631, 10.5194/acp-13-10609-2013, 2013.

Table 1. Locations, time periods and used datasets of five field campaigns

Location	Wuqing	Wuqing	Xianghe	Wangdu	Gucheng
Time period	7 march to 4 April, 2009	12 July to 14 August, 2009	9 July to 8 August, 2013	4 June to 14 July, 2014	15 October to 25 November, 2016
PNSD	TSMPS+APS	TSMPS+APS	TSMPS+APS	TSMPS+APS	SMPS+APS
BC	MAAP	MAAP	MAAP	MAAP	AE33
σ_{sp}	TSI 3563	TSI 3563	TSI 3563	TSI 3563	Aurora 3000
f(RH)				Humidified nephelometer system	Humidified nephelometer system
g(RH)				HH-TDMA	

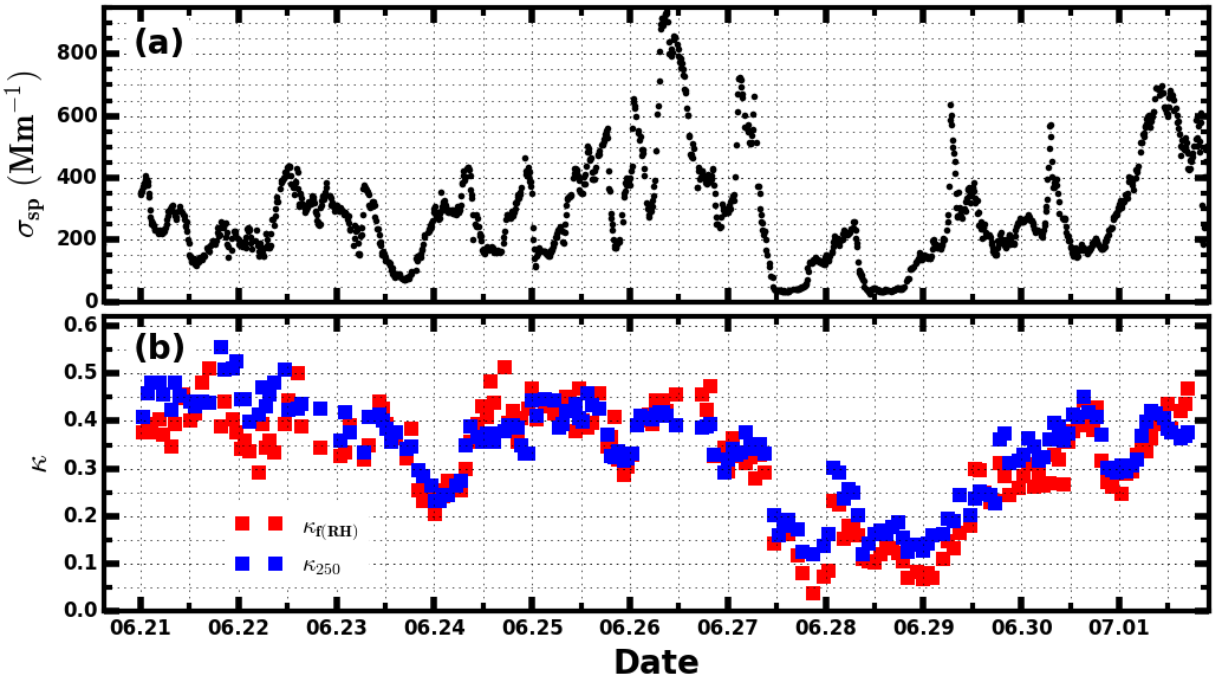

Figure 1. (a) The time series of σ_{sp} at 550 nm; (b) The time series of κ values derived from $f(\mathrm{RH})$ measurements ($\kappa_{f(\mathrm{RH})}$) by combining information of PNSD and BC, and time series of average κ values of aerosol particles at 250 nm (κ_{250}) which is calculated from measurements of HH-TDMA.

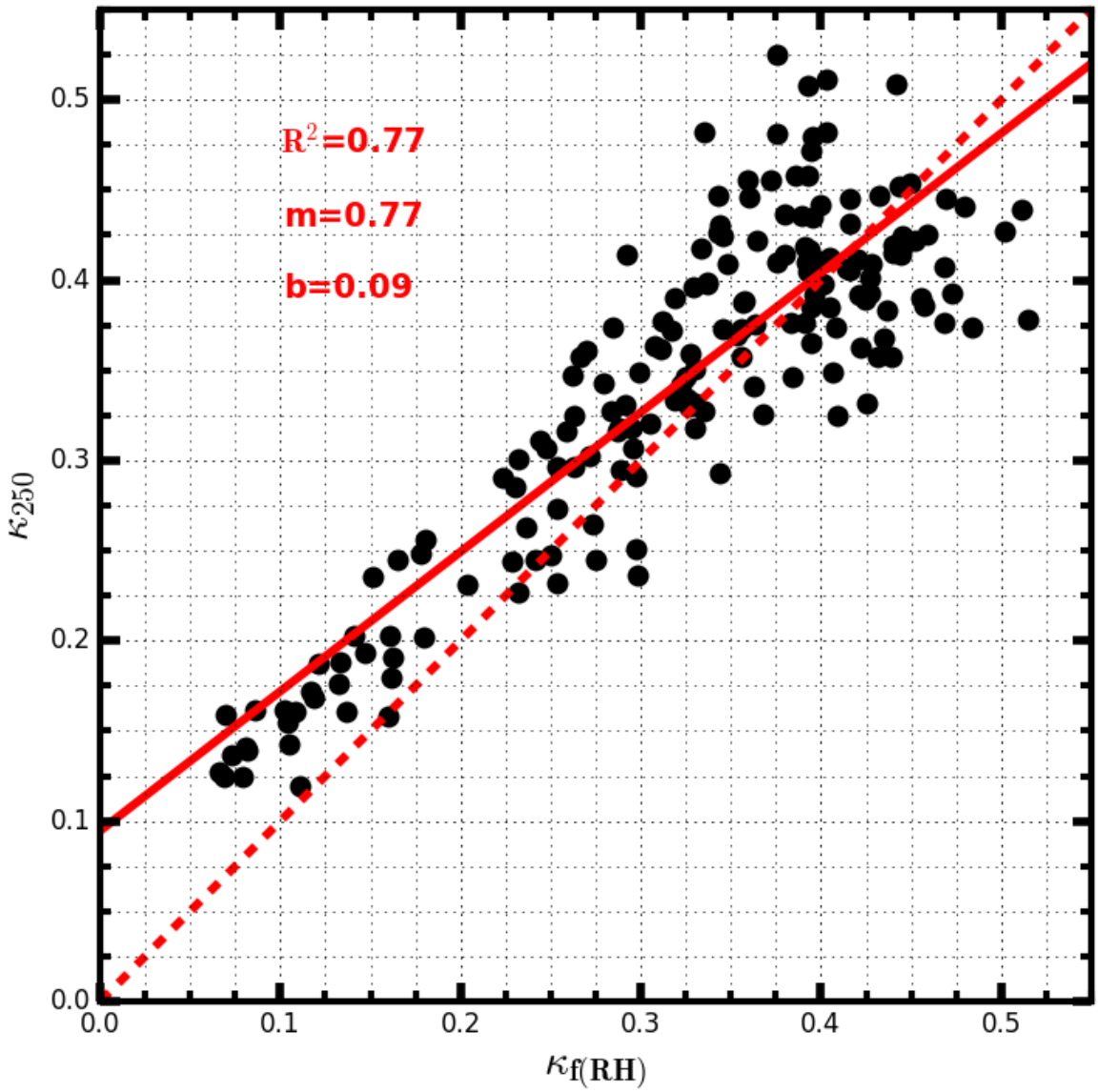

Figure 2. The comparison between κ values derived from $f(\mathrm{RH})$ measurements ($\kappa_{f(\mathrm{RH})}$) and average κ values for aerosol particles with a diameter of 250 nm (κ_{250}) which are derived from measurements of HH-TDMA. R^2 is the square of correlation coefficient, m is the slope and b is the intercept.

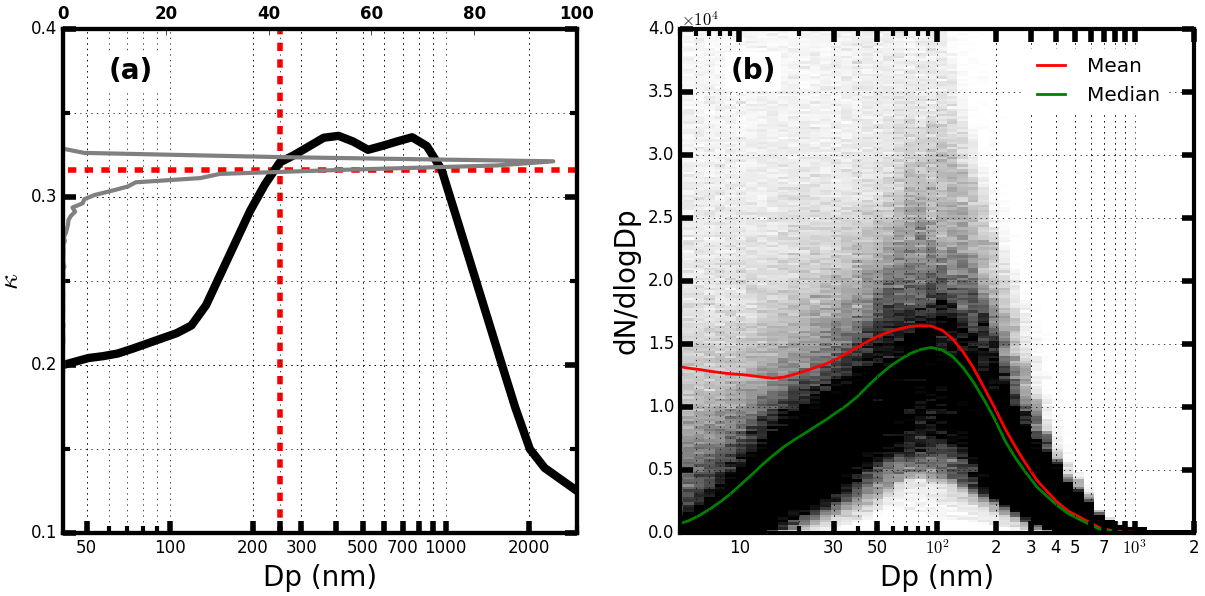

Figure 3. (a) The thick black line represents the average size-resolved κ distribution from HaChi campaign. The solid gray line represents the probability distribution of retrieved κ values with this size-resolve κ distribution by using all PNSDs shown in figure (b), and the horizontal dashed line represents their average. The vertical dashed red line represents the position of 250 nm. (b) All PNSDs which are observed from three different representative background sites of the NCP during summer, they are used to model relationship between size-resolved $\kappa$and retrieved κ values from $f(\mathrm{RH})$ measurements, and the gray color represents the frequency of PNSD, darker point corresponds to higher frequency, red and green line represent mean of median values of all observed PNSDs.

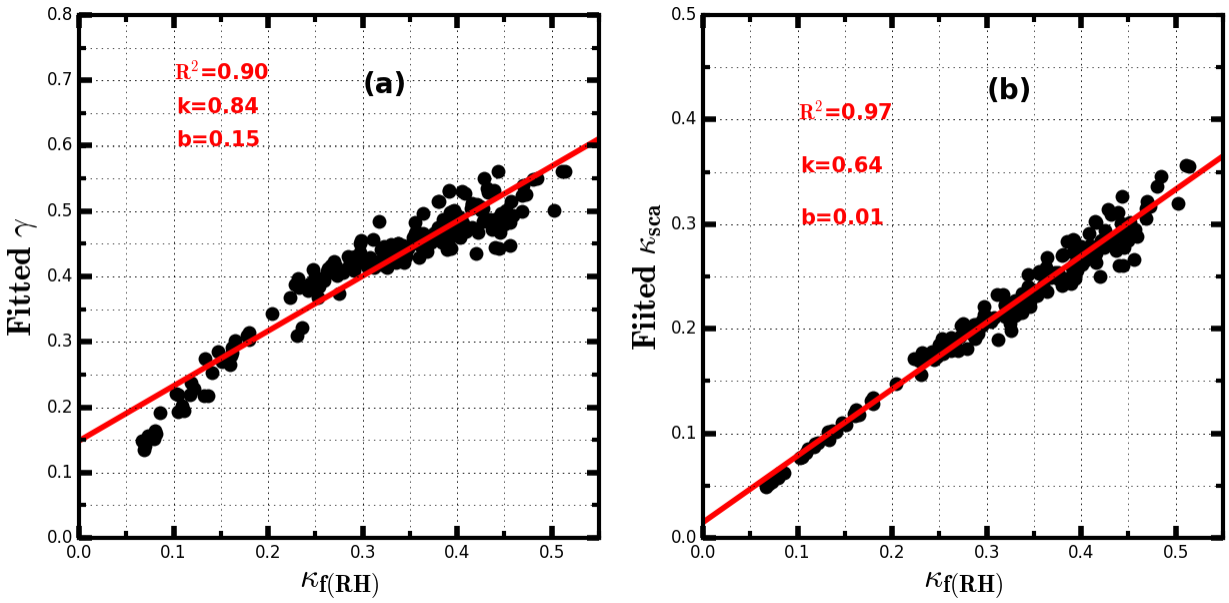

Figure 4. (a) The linear relationship between values of $\kappa_{f(\mathrm{RH})}$ and fitted γ, R^2 is the square of correlation coefficient, k is the slope and b is the intercept; (b) The linear relationship between values of $\kappa_{f(\mathrm{RH})}$ and fitted κ_{sca}.

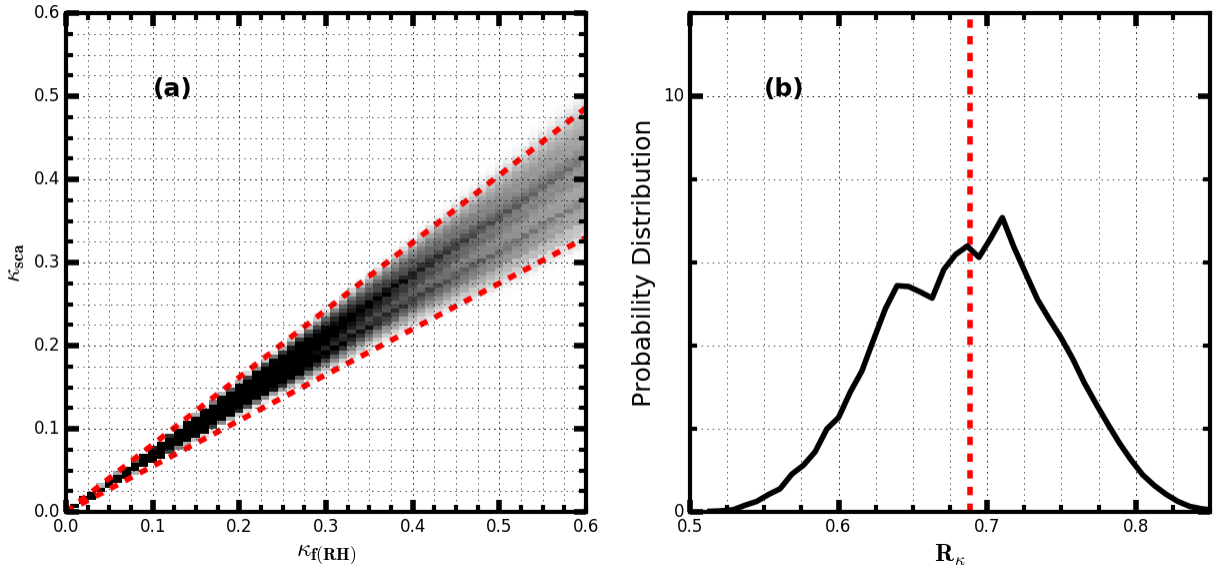

Figure 5. (a) Simulated relationships between $\kappa_{f(\mathrm{RH})}$ and κ_{sca} under different PNSD conditions (all PNSDs shown in Fig.3a are used as inputs to conduct the simulation experiment), gray color represents the frequency and darker point corresponds to higher frequency, the slope of two dashed lines are 0.55 and 0.81; (b) The probability distribution of R_κ $(\kappa_{sca}/\kappa_{f(\mathrm{RH})})$.

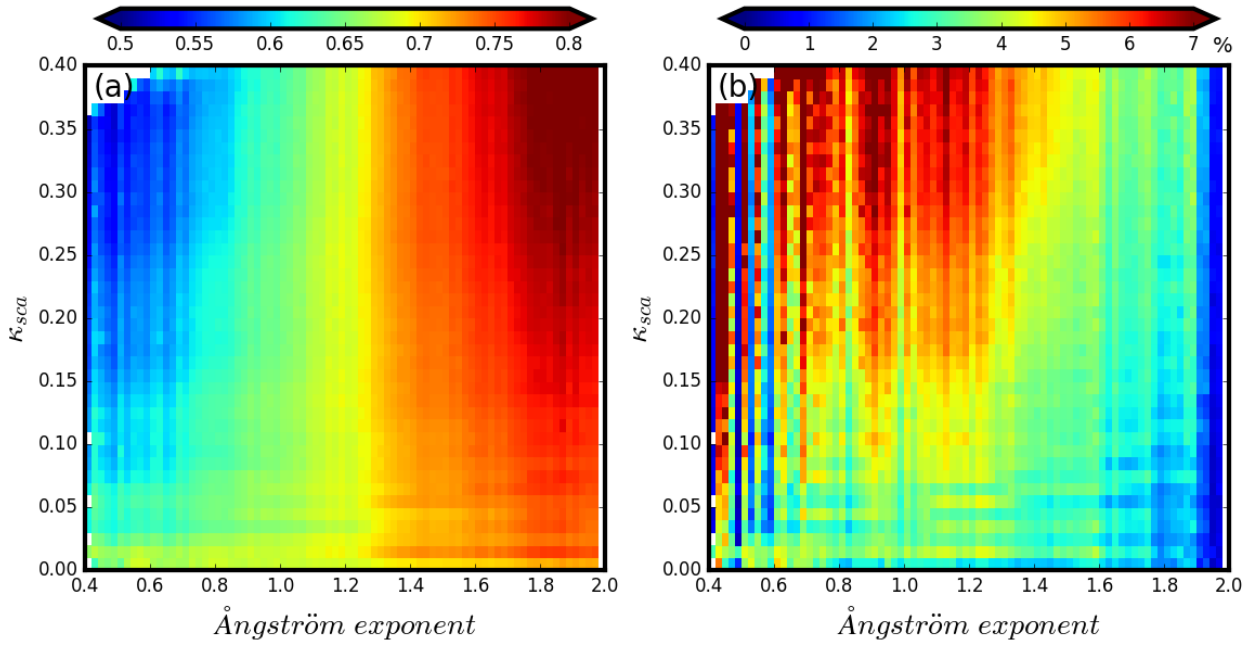

Figure 6. (a) Colors represent R_κ values and the color bar is shown on the top of this figure, x-axis represents Ångström exponent and y-axis represents κ_{sca}. (b) Meanings of x-axis and y-axis are same with them in (a), however, color represents the percentile value of the standard deviation of R_κ values within each grid divided by their average.

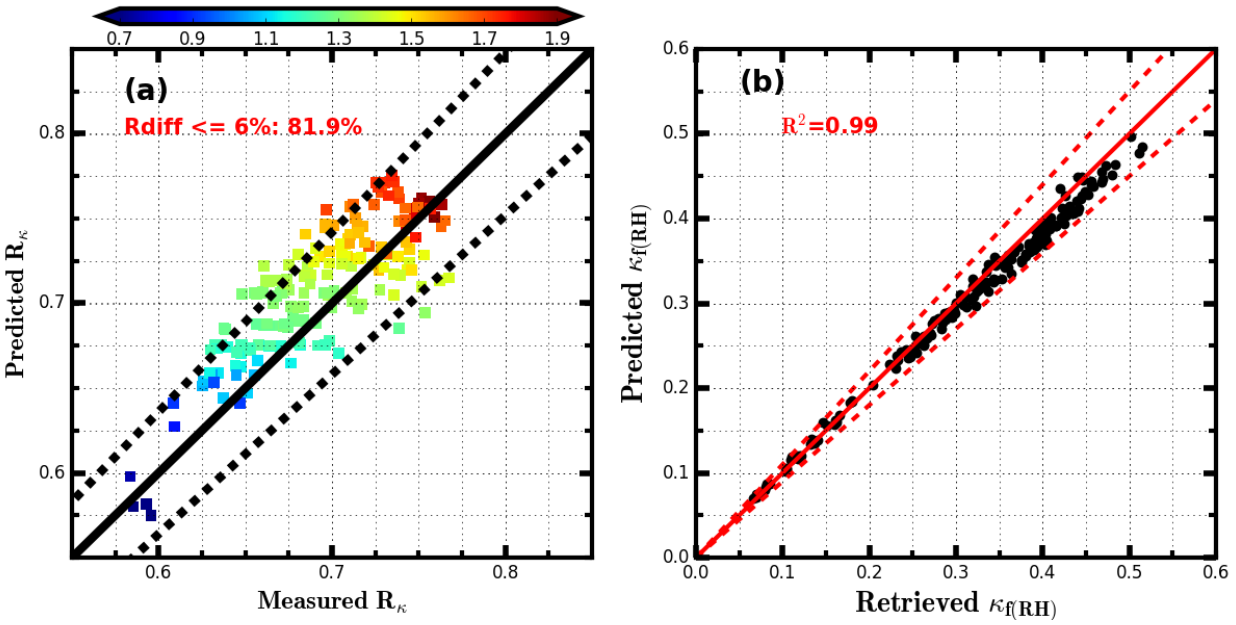

Figure 7. (a) The comparison between measured and predicted R_κ values, colors represent values of Ångström exponent, texts with red color show the percentile of points with relative difference (Rdiff) less than 6% , two dashed line are 6% relative difference lines ; (b) the comparison between $\kappa_{f(\mathrm{RH})}$ retrieved from Method 1 and predicted $\kappa_{f(\mathrm{RH})}$ by using the new method introduced in Sect.4.3, R^2 is the square of correlation coefficient, two dashed lines are 10% relative difference lines.

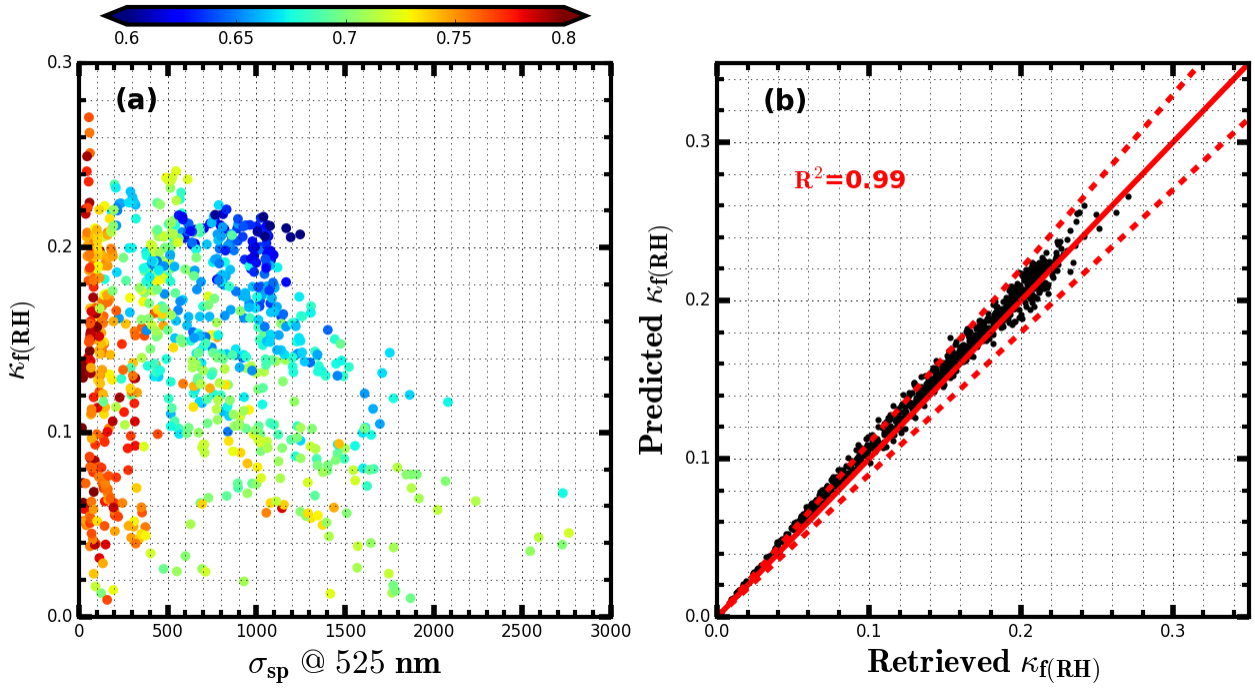

Figure 8. (a) x axis represents σ_{sp} at 525 nm (Mm^{-1}), y axis represents retrieved $\kappa_{f(\mathrm{RH})}$, colors of scatter points represent corresponding values of R_κ; (b) The comparison between $\kappa_{f(\mathrm{RH})}$ retrieved from Method 1 and predicted $\kappa_{f(\mathrm{RH})}$ by using the new method, R^2 is the square of correlation coefficient, two dashed red lines represent 10% deviations from 1:1 line.